EUROPHYSICS LETTERS 10 January 1997

Europhys. Lett., **37** (2), pp. 133-138 (1997)

Soft–X-ray fluorescence of porous silicon: electronic structure of Si nanostructures

S. EISEBITT[1,2], S. N. PATITSAS[2], J. LÜNING[1], J.-E. RUBENSSON[1]
T. TIEDJE[2,3], T. VAN BUUREN[2] and W. EBERHARDT[1]

[1] *Institut für Festkörperforschung, Forschungszentrum Jülich*
D-52425 Jülich, Germany
[2] *Department of Physics, University of British Columbia*
Vancouver, BC, V6T 1Z1, Canada
[3] *Department of Electrical Engineering, University of British Columbia*
Vancouver, BC, V6T 1Z1, Canada

(received 8 March 1996; accepted in final form 29 November 1996)

PACS. 73.20Dx – Electron states in low-dimensional structures (including quantum wells, superlattices, layer structures, and intercalation compounds).
PACS. 71.20Mq – Elemental semiconductors.
PACS. 71.20–b – Electron density of states.

Abstract. – The electronic structure of porous Si is investigated using soft–X-ray fluorescence spectroscopy. Significant changes are observed as compared to bulk Si, which we interpret as due to altered electronic structure in the Si nanostructures. By imposing standing wave boundary conditions on the valence band wave functions, we calculate the fluorescence spectrum for thin Si sheets of different orientations. For a (100)-oriented sheet, the calculation is in good agreement with the experimental spectra, suggesting that the nanostructure in porous Si is predominantly in the form of thin Si (100)-type sheets.

Nanosized structures differ in a variety of physical properties from their bulk counterparts. In particular the electronic structure can be altered in small particles. This change is in part due to the increasing influence of the *surface* with its different electronic structure, but also due to the fact that the electrons in the *bulk* of the material experience the confinement in a small structure when the size of the structure becomes comparable to electron wavelengths. While the electronic structure of surfaces has been studied extensively, less work has so far been dedicated to the investigation of the bulk electronic structure of small particles.

Porous silicon is a material that has recently attracted considerable interest because of its room temperature luminescence. It is now generally agreed that the presence of nanosized Si structures in this material is essential for its light-emitting properties [1]. While scanning electron microscopy gives some insight into the structural properties of porous Si on lengthscales ranging from 20 nm to macroscopic dimensions [2], little is known about the structure on lengthscales of a few nanometers, *i.e.* on lengthscales where quantum confinement of the electronic states is to be expected. Early theoretical work focussed on wire-like structures,

© Les Editions de Physique

while recently planar Si structures have been suggested to be connected to the unusual optical properties of porous Si [3], [4]. In this paper we show for the first time that it is possible to obtain detailed information about the geometry of nanostructures from soft–X-ray fluorescence (SXF) spectra.

We have measured the spectral distribution of the fluorescence radiation generated in transitions of Si VB electrons to the Si $2p_{3/2}$ core level where a vacancy has been selectively generated using monochromatized synchrotron radiation. SXF was excited with radiation from the BW3 undulator beamline at HASYLAB [5], and analyzed in a spherical grating grazing-incidence Rowland spectrometer using a 3710 mm grating with 600 lines/mm and a 30 μm entrance slit. Due to the photon-in–photon-out type of process, the experiment overcomes the sample charging problems often encountered by electron spectroscopies on electrically not well connected samples.

We compare the experimental results with calculations of the SXF spectrum obtained for planar Si model structures with different orientations. As we will see below, the calculated SXF spectra are significantly different for the different orientations and hence structural information can be obtained from the comparison of experiment and theory.

In fig. 1*a*) we present the SXF spectrum from a (100) Si wafer excited at 100.00 eV photon energy and recorded with a resolution of 250 meV. The bandwidth of the synchrotron radiation for excitation was set to 100 meV, allowing us to selectively create Si $2p_{3/2}$ vacancies. For excitation energies not close to an absorption edge, the Si SXF spectrum with its three pronounced peaks has been successfully interpreted in terms of the symmetry selected density of states (DOS) locally at the Si atom [6] (1).

In fig. 1*b*), *c*) we present a calculation of the bulk Si SXF spectrum. We have computed the Si fluorescence spectrum in the following way: first we calculate the Si band structure using a LCAO approach including up to third-neighbor interactions [9]. The SXF spectrum is then calculated taking the on-site and off-site dipole overlaps of the valence electron wave functions with the $2p_{3/2}$ core orbitals into account. In order to obtain the overlaps correctly, the shape of the valence band wave function in the vicinity of the atomic *core* has to be known [6]. However, the exact shape of the valence wave function close to the core is not required in most band structure calculations and small deviations can produce significant errors in the overlap integral with the core level. Therefore, we have treated the magnitude of the s-like and p-like offsite overlap as (the only) free parameters in the calculation (2). The calculated spectrum is broadened to account for the initial- and final-state lifetimes and the experimental resolution (3). As seen in fig. 1*a*), *b*) the tight-binding calculation is in reasonable agreement with the experiment.

The experimental SXF spectrum of porous Si is compared to the bulk Si spectrum in fig.1*a*). Porous Si samples were prepared by anodizing n-type (100) Si wafers under front side

---

(1) In order to minimize effects due to momentum conservation in the absorption-emission process [7], [8] while still obtaining spin-orbit separation, we avoid high symmetry points in the band structure by exciting the $2p_{3/2}$ electrons into states about 0.25 eV above the conduction band minimum.

(2) In the calculation the $2p$ core orbital dipole matrix element was replaced by a symmetric $3s$ orbital overlap with no dipole term. The values we used for the overlaps of a $3s$ orbital with first-, second- and third-nearest-neighbor $3s$ orbitals, respectively, are 0.053, 0.009, 0.0002, all values scaled together by one free parameter. The analogous numbers used for the $3p_x$ orbitals are -0.501, -0.174, -0.110 (311 direction), -0.037 (113 direction) again scaled together.

(3) Type and full width at half-maximum of the broadening functions used are as follows: initial state, Lorentzian, 0.09 eV [6], [10]; final state, Lorentzian, whose width is energy dependent. The width was calculated by computing the Auger decay probability from the DOS, neglecting matrix element effects. Instrumental resolution: Gaussian, 0.25 eV.

illumination ([4]). Si $L_{2,3}$ absorption spectra exhibit a shift of the conduction band (CB) edge of 0.18 eV for the sample shown as compared to bulk Si. The excitation energy for the SXF spectrum was therefore set to $h\nu$ =100.20 eV in order to excite into states about 0.25 eV above the CB minimum, as in the bulk Si case. Photoluminescence from the porous Si was visible *in situ* under the 100 eV photon excitation.

The SXF spectrum of porous Si exhibits the same overall three-peak structure typical of the spectrum of bulk crystalline Si, indicating that we are mainly probing crystalline-like material rather than amorphous Si, which has a distinctly different SXF spectrum [7]. Although the overall spectral shape is similar for bulk and porous Si, clear differences between the two materials are observed in the whole spectral region from the VB edge down to about 11 eV below the edge. The VB band edge is found to be shifted to lower energy by 0.54 ± 0.05 eV. This shift is consistent with the quantum confinement model for porous Si. Similar VB edge shifts have been reported from electron spectroscopy experiments [11].

The VB edge as seen in the porous Si SXF spectrum is *steeper* than in the Si spectrum. This slope increase is due to a larger DOS at around -2.5 eV in the porous Si in conjunction with the VB edge shift. Deeper in the band, we observe a higher intensity for the porous Si between -4 eV and -7 eV and a lower intensity in the adjacent region between -7 eV and -11 eV. The position of peak B is shifted 0.15 eV towards higher energies in porous Si. The same changes in the shape of the DOS have been observed in the SXF spectra of all samples investigated with VB edge shifts ranging from 0.54 eV to 0.70 eV depending on the preparation conditions [12]. As we expect some broadening of these spectral changes due to the size and shape distributions of Si nanostructures in the porous Si, we note that the fact that the slope of the VB edge in porous Si *increases* indicates that the DOS change at the top of the VB in the small Si structures is large compared to the inhomogeneous broadening.

While it is a theoretical challenge to calculate the electronic structure and the fluorescence spectrum of Si nanostructures taking different shapes and crystal orientations into account, we can explore the effects of nanocrystal orientation and size with a simple model. We assume the nanostructures to be (100), (110) or (111)-oriented Si sheets. The electron confinement in the thin Si sheets is modeled by restricting the component of the electron wavevector $k_\perp$ perpendicular to the Si sheets to certain discrete values that satisfy the boundary conditions for electron standing waves imposed by the confinement in one dimension. We neglect any $k_{\parallel}$ dependence of the boundary conditions which define the allowed values for $k_\perp$. This means the allowed **k**-states used in the calculation form parallel planes in reciprocal space. These planes are equally spaced throughout **k**-space except that the plane passing through the origin, and all symmetrically equivalent planes are excluded. The exclusion is due to the boundary conditions causing the wavefunction to be zero when **k** is on such planes. This treatment is analogous to the calculation of the electronic states for a finite chain of atoms, and extrapolates to the effective mass result for the quantum shift of the band edge, for thick sheets. (A similar "truncated crystal" approach has been shown to reproduce results of pseudopotential calculations for thin Si films [13]. The envelope functions of the occupied electronic bulk states were reported to be rather insensitive on the degree of hydrogenation, if no dangling bonds are present [14].) In order to calculate the fluorescence spectrum for the Si sheets, the $k_\perp$-restriction is applied to the same LCAO band structure which was used for the bulk Si case, using the same overlap and broadening parameters.

In fig. 1 *b*), *c*) we compare the calculated fluorescence spectra for bulk Si with the Si sheet spectra for (100) and (110) orientations. The $k_\perp$ values used are $\pm \frac{1}{2}\frac{2\pi}{a}(100)$ in the (100)

([4]) The anodization was carried out in a 1:1:2 HF : H_2O : ethanol solution with 5 V between the Pt electrode (−) and the back of the silicon substrate (+). The current density was 22.3 mA/cm^2. Samples were exposed to air for less than 3 min prior to loading into the UHV chamber.

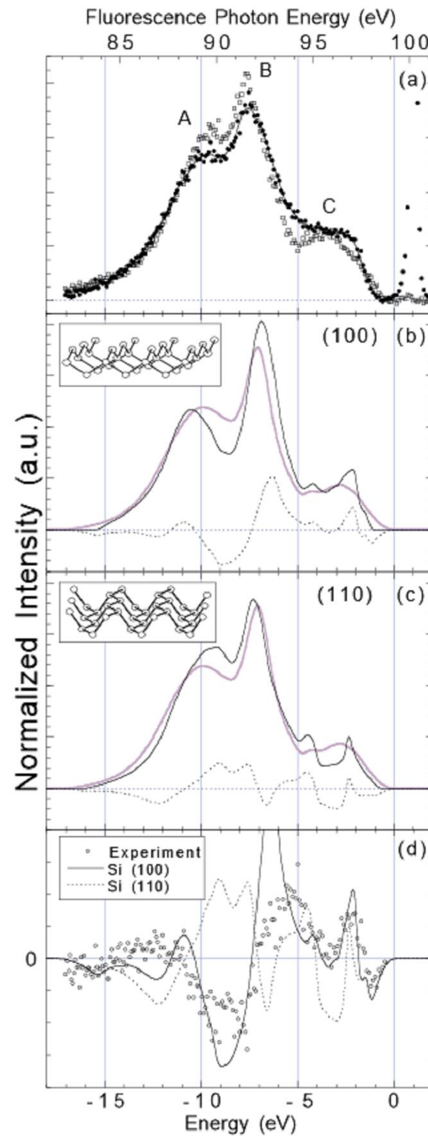

Fig. 1. – *a*) Normalized soft–X-ray fluorescence spectra of bulk Si (open squares) and porous Si (filled circles, with smooth line to guide the eye) excited with photons of 100.00 eV and 100.20 eV, respectively. The SXF spectra are divided by the cube of the fluorescence energy to facilitate comparison with the DOS. An approximate Fermi energy scale has been introduced for comparison with theory (bottom). The (clipped) peak around 100 eV is due to diffuse reflection of the primary beam into the spectrometer. It is intense on the rough porous Si sample and weak on the polished bulk Si wafer. *b*), *c*) Calculated fluorescence spectra for bulk Si (wide grey line) and Si sheets (thin black line) for Si(100) (*b*) and Si(110) (*c*). The respective difference spectra are shown as dashed lines. In the insets we show schematics of the Si sheets used in the model. *d*) Experimental SXF difference spectrum of porous and bulk Si from the data in panel *a*) (circles) compared to the theoretical difference spectra for the Si(100) (solid line) and Si(110) (dashed line) thin layer models. All spectra in *a*)–*c*) are normalized to unity VB area.

case, $\pm\frac{1}{3}\frac{2\pi}{a}(110)$ and $\pm\frac{2}{3}\frac{2\pi}{a}(110)$ in the (110) case and $\pm\frac{1}{3}\frac{\pi}{a}(111)$ and $\pm\frac{\pi}{a}(111)$ in the (111) case (not shown). These $k_\perp$ values correspond to the thinnest connected sheets in the three orientations. Even with the inclusion of lifetime broadening and experimental broadening, the calculated SXF spectra for the different Si nanostructures are significantly different from each other and the bulk Si spectrum.

In order to compare the experimental data with the calculations, we present difference spectra in fig. 1 *d*). For the Si (100) sheet the calculated difference spectrum reproduces the experimental one rather well, including the shift and steepening of the VB edge. The calculation reproduces the experimental differences from the VB edge down to -5 eV, and the minimum around -9 eV as far as the energy positions and the intensities of the difference spectra are concerned. The only spectral feature not reproduced quantitatively by the theory is the maximum at -6 eV, although the calculation does reproduce the 0.2 eV shift to higher energy of peak B. In contrast, the difference spectra derived from Si (110) tends to be anticorrelated with the experimental data. (The calculation for Si (111), which is not shown, is an even worse match to the data.) To quantify the agreement with the experimental data for the three model structures, we define a correlation coefficient equal to the integral of the product of the experimental and calculated difference spectra, normalized by the average of the squares of the difference spectra. This figure of merit is one, when the two data sets are identical, zero when they are uncorrelated, and minus one when anticorrelated. The figures of merit for the (100), (110) and (111) model calculations are 0.7, -0.5 and 0.1, respectively. This analysis confirms that the experimental data is described rather well by the Si (100) sheet calculation.

States associated with surface hydrogen could also contribute to the experimental difference spectra, since we expect the porous Si surface to be terminated with hydrogen. The dominant feature in the VB DOS due to Si-H bonds is believed to be a peak at -5.5 eV [15], [4]. Although the experimental difference spectrum has a peak at this energy, the other features at -1 eV, -2 eV, and -9 eV are not consistent with Si-H bonds, whereas they match the Si (100) sheet calculation rather well.

The agreement between the experimental data and the Si(100) calculation is good given the well-known limitations of LCAO theory. This suggests that the nanostructures in porous Si are in the form of thin Si sheets, oriented perpendicular to (100), (010) or (001) on a nanometer lengthscale. As these directions are mutually perpendicular, the (100)-type sheets can be arranged to form a three-dimensional network. We clearly cannot rule out the possibility that some other structures might give as good or better agreement with the experimental data, since we have only checked three different structural models. However, more elaborate electronic structure calculations will be needed to resolve this issue.

Recently, the microscopic structure of PS samples has been investigated by various spectroscopic methods such as EXAFS [16] or polarization-dependent PL spectroscopy [17]. We want to point out that the results obtained in these experiments refer to different length scales and probing depths. EXAFS is probing the immediate surrounding of nearest- and next-nearest-neighbor shells. Our SXF results and the electronic structure data have a relevant length scale of about 30 A in diameter and probe specifically the PS within the topmost 1000 A of the sample, while the luminescence studies probe almost the entire bulk of the sample.

From the results presented above, we rule out (110) and (111)-oriented thin Si sheets as candidates for a common form of nanostructure in porous Si. The observation of a preferred crystallographic orientation is not surprising since the etching process of n-type porous Si is known to be anisotropic. Even for non-(100) wafers or various orientations of the etch current lines to the crystallographic directions, the etching reaction proceeds preferentially in (100) directions as the F induced weakening of the Si backbonds is strongest for a Si (100)

surface [2], [3], [18].

In conclusion, we have observed significant changes in the VB band DOS of porous Si as compared to bulk Si which extend deep into the band and are visible in the SXF spectra down to -11 eV. We attribute the observed changes in the fluorescence spectrum to changes in the electronic band structure associated with standing wave boundary conditions for the valence band wave functions in planar Si nanostructures. Comparison of experiment and theory indicates that the SXF spectrum is sensitive to the detailed nanostructure of porous Si. We show that the observed spectra are in good agreement with the nanostructures, being very thin (100)-oriented Si sheets.

***

We thank T. MÖLLER, O. BJÖRNEHOLM, S. KAKAR, F. FEDERMAN, and A. RIECK for their help at the beamline and D. A. PAPACONSTANTOPOULOS for the use of his LCAO code. We thank DAAD and NSERC for financial support.

REFERENCES

[1] BRUS L., HIROSE M., COLLINS R. W., KOCH F. and TSAI C. C., (Editors), *Microcrystalline and Nanocrystalline Semiconductors*, *Mater. Res. Soc. Proc.*, **358** (MRS, Pittsburgh) 1995.
[2] LEHMANN V., *J. Electrochem. Soc.*, **140** (1993) 2836.
[3] LEHMANN V. and GÖSELE U., *Appl. Phys. Lett.*, **58** (1990) 856.
[4] TSE J. S., DAHN J. R. and BUDA F., *J. Phys. Chem.*, **99** (1995) 1896.
[5] LARSSON C. *et al.*, *Nucl. Instrum. Methods A*, **6** (1994) 1172.
[6] KLIMA J., *J. Phys. C*, **3** (1970) 70.
[7] MIYANO K. E. *et al.*, *Phys. Rev. B*, **48** (1993) 1918.
[8] MA Y., *Phys. Rev. B*, **49** (1994) 5799.
[9] PAPACONSTANTOPOULOS D. A., *Handbook of the Band Structure of Elemental Solids* (Plenum, New York, N.Y.) 1986.
[10] O'BRIEN W. L. *et al.*, *Phys. Rev. B*, **47** (1993) 140.
[11] VAN BUUREN T. *et al.*, *Appl. Phys. Lett.*, **63** (1993) 2911; VAN BUUREN T. *et al.*, *Phys. Rev. B*, **50** (1994) 2719.
[12] EISEBITT S. *et al.*, *Solid State Commun.*, **97** (1996) 549.
[13] ZHANG S. B., YEH C.-Y. and ZUNGER A., *Phys. Rev. B*, **48** (1993) 11204.
[14] GAVRILENKO V. I. and KOCH F., *J. Appl. Phys.*, **77** (1995) 3288; UDA T. and HIRAO M., *J. Phys. Soc. Jpn. Suppl. B*, **63** (1994) 97.
[15] ALLAN D. and JOANNOPOULOS J. D., in *Hydrogenated Amorphous Silicon II*, *Topics in Applied Physics*, **56** (Springer, Berlin) 1984.
[16] SCHUPPLER S. *et al.*, *Phys. Rev. Lett.*, **72** (1994) 2648.
[17] KOVALEV D. *et al.*, *Appl. Phys. Lett.*, **67** (1995) 1585.
[18] CHUANG S.-F. *et al.*, *Appl. Phys. Lett.*, **55** (1989) 675.